Accepted to Phys. Fluids 10.1063/5.0170486

APS/123-QED

Wide flow model for converging gravity currents and the effects of the flow resistance model on the propagation

S. Longo

Department of Engineering and Architecture - Università degli Studi di Parma - Parco Area delle Scienze 181/A - 43124 Parma - Italy[a]

(Dated: 16 September 2023)

We are investigating flows in the viscous-buoyancy balance regime in a converging channel with a cross-section described by a power function $y =\sim x^k z^r$, where x and y are the streamwise and spanwise horizontal coordinates, respectively, and z is the vertical coordinate. We are interested in the different results depending on whether we use a simplified model of the flow resistance law, which varies depending on whether the height of the current is much greater/smaller than the channel width, or a somewhat more general model described by the Darcy-Weisbach equation in which the flow resistance law depends on the shape of the cross-section through the Fanning friction factor. The simplified models, one of which developed here is original and new, allow a self-similar solution of the second kind, unlike the general model. The general model, to the best of our knowledge applied for the first time to a generic cross-section described by a power function, requires numerical integration. However, a comparison of the front propagation of the gravity current according to the different models, performed by numerical integration of the differential problem, shows that the current assumes a self-similar arrangement as a good approximation for the general model. For some channel geometries, the three models give a very similar result, which results in a difficult attribution to a specific model based on experiments. The effects of anisotropy in the vertical direction of the channel cross-section are also highlighted by both the numerical and self-similar solutions.

[a] https://sandro.longo.unipr.it/

Accepted to Phys. Fluids 10.1063/5.0170486

I. INTRODUCTION

Gravity currents (GCs), generated mainly by density differences of various kinds occurring in a flow domain, are a model for a wide range of natural phenomena and industrial processes for which the geometric and temporal scales are, to some extent, in a similarity condition. This condition favours mathematical description framing in problems that admit families of solutions. Geometric homotheticity, accompanied by temporal scaling, guarantees the possibility of reducing the number of variables involved with self-similar solutions. These are approximate solutions, reproducing some essential elements of the propagation process while neglecting other effects that play a role either in the initial stage or in the final stage. The pioneering analysis of Barenblatt[1] introduced the concept of “intermediate asymptotics”, i.e., asymptotics that are not valid too early or too late, but only in an intermediate interval. See also Longo[2] for a description of the principles behind this concept.

The availability of solutions, albeit approximate but known either analytically, or with the possibility of extracting some relevant properties of the physical process, such as the dependence of the front position on time, and the dependence of the current profile on space, allows analysis with very synthetic results that facilitate comparison with field experiments and ultimately simplify the interpretation. The book by Ungarish[3] details several models of GCs grouped into classes and sharing the kind of the solution.

The two main families of self-similar solutions are of the first kind and of the second kind, where the dimensional arguments in the former allow the identification of the self-similar variables, and the self-similar variables in the latter are identified only a posteriori, after the problem has been solved. For example, solutions for the propagation of two-dimensional and axisymmetric viscous GCs belong to the first family[4]. The second family includes convergent gravity flows (in addition to numerous other phenomena), analysed according to the scheme originally proposed by Gratton & Minotti[5] and later extended to reproduce spatial variability in the properties of porous media[6] or to account for drainage through a permeable substrate[7]. Other analyses of second-kind self-similar solutions have been previously provided by scholars[8–15]. The review in Zheng & Stone[16] provides a detailed overview of the most relevant contributions.

The proper use of self-similar solutions requires knowledge of their degree of approximation, and of the extension of the interval defined as “intermediate asymptotic”. In this respect, both the experimental measurements of Zheng *et al.*[6] and Longo *et al.*[15] and the numerical analyses in Ball *et al.*[17], Ball & Huppert[18] help to explore these aspects in more detail. However, the approximation of the solution is also compounded by the approximation of the model adopted, which makes it more difficult to identify deviations from the experimental results; the effects of capillarity, the curvature of the trajectories, the approximation adopted in the description of the flow field and the rheology of the fluid (for non-Newtonian fluids) are among these approximations.

In detail, the flow of a current in a viscous regime in a channel with boundaries expressed by a power function can be computed by considering (i) the tangential stresses in the vertical planes to be dominant, if the width of the current is small compared to its height; (ii) the tangential stresses in the horizontal planes to be dominant, if the height of the current is small compared to its width[19]; and (iii) the tangential stresses in both horizontal and vertical planes to be relevant. For the sake of simplicity, Case (i) will be referred to as the "narrow flow model", Case (ii) as the "wide flow model", and Case (iii) as the "general model". This nomenclature indicates that, for example, in fractures the narrow flow model is preferentially, but not exclusively, the most appropriate model: even in fractures close to the GC front where the height is of the same order as the width, the narrow flow model is only approximated. It is also understood that the general model is the most extensive of the three models although in the present analysis we neglect the variability of the Fanning coefficient as the filling level of the cross-section varies, as will be made explicit in the §II.

While the differential problems resulting from the different approximations are similar, the numerical outcomes are different, and some aspects of the current propagation lead to different conclusions; we expect that a more general description of the flow field, relaxing some approximations, may lead to a differential problem without self-similar solutions.

In this article, we will focus on these aspects, while also considering other aspects that generalize the previous literature. We include the variability of the domain in the vertical direction, which introduces a further degree of anisotropy to that represented by the convergence of the channel in the direction of flow. The analysis is carried out for converging flows of a Newtonian fluid in channels with geometry described by power functions.

The manuscript is structured as follows. The model and the different flow resistance laws are described in §II. In §II B, we introduce the self-similar solution identification procedure for the case of a wide flow model, and in §II C, there is a description of the differential

Accepted to Phys. Fluids 10.1063/5.0170486

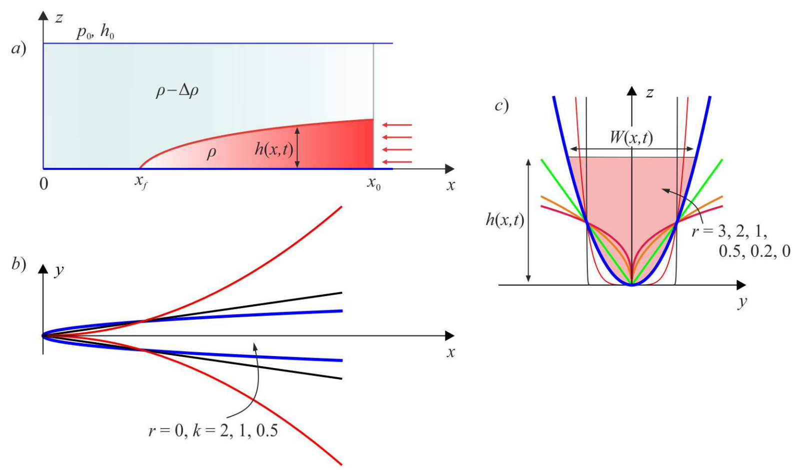

FIG. 1. Schematic of a GC advancing towards the origin in a channel with boundaries described by the function $y = \pm(b_0/2)x^k z^r$, with a gap width $b = 2|y| \equiv b_0 x^k z^r$ and a top width of the current $W(x,t) = b(x, h(x,t))$. *a)* Side view, *b)* top view, and *c)* cross-section.

problem and of the finite difference procedure for the case of a general model. In §III, we compare the results for the different flow resistance laws. Section IV contains the summary and the conclusions. The Appendix briefly describes the differential problem for the narrow flow model.

II. THEORY

A. Formulation of the model

We consider a horizontal channel with a rigid-walled, impermeable cross-section described by a power function $y = \pm(b_0/2)x^k z^r$, where b_0 is a parameter of dimension $[b_0] = L^{1-k-r}$ controlling the width, and k and r are two dimensionless parameters controlling the variation in the streamwise x direction and in the vertical direction z, respectively; see the schematic in figure 1.

A positive value of k indicates a divergent channel in the horizontal, which widens as x increases; values of $0 < r < 1$ and $r > 1$ control the variation of the gap width in the vertical direction, and correspond to a narrow fracture and a wide channel, respectively. As special cases, $r = 0$ corresponds to a rectangular section of width $b_0 x^k$; $r = 1/2$ corresponds to a parabola in general, and to a circular cross-section of radius $b_0^2 x^{2k}/8$ if the current width is smaller than the radius; $r = 1$ corresponds to a symmetrical triangular section, which is wide/narrow for large/small values of $b_0 x^k$. We assume that the streamflow variation of the cross-section is such that the component of stresses normal to the wall in the flow direction is negligible , and that the geometric scale along x is much larger than the geometric scales along y and z. Furthermore, the variations in the variables in the transverse y direction are zero, with a uniform sharp interface between the current and the ambient fluid in the y direction and with negligible effects of the surface tension. The viscosity of the intruding fluid is higher than the viscosity of the ambient fluid, and we do not expect Saffman-Taylor instabilities.

We assume the classical Newtonian relation between shear stress and shear rate:

$$\tau = \mu \dot{\gamma}, \tag{1}$$

where τ is the tangential stress, $\dot{\gamma}$ is the strain rate and μ is the viscosity.

Neglecting capillary effects and the curvature of the streamlines, the pressure within the current fluid domain is $p = p_0 + (\rho - \Delta\rho) g (h_0 - h) + \rho g (h - z)$, $0 < z < h$, where g is gravity and p_0 is the pressure in the ambient fluid at $z = h_0$, assumed to be constant. For low Reynolds number flows, we can neglect the inertial effects, and the balance is between the relevant normal and tangential stresses; hence,

$$\frac{\partial \tau_{zx}}{\partial z} + \frac{\partial \tau_{yx}}{\partial y} + \frac{\partial p}{\partial x} = 0, \tag{2}$$

with a driving pressure gradient equal to

$$\frac{\partial p}{\partial x} = \Delta\rho \, g \frac{\partial h}{\partial x}. \tag{3}$$

At this point, we generally proceed by assuming that in the case of currents with a height h much greater than the width W, with $h \gg W$ (narrow flow model), the horizontal dynamics dominate since $\partial \tau_{yx}/\partial y \gg \partial \tau_{zx}/\partial z$; in the opposite case, if $h \ll W$ (wide flow model), the vertical dynamics dominate since $\partial \tau_{yx}/\partial y \ll \partial \tau_{zx}/\partial z$. This simplifies eq. (2), allowing direct integration of the velocity field. In the first case, for the narrow flow model, the streamwise velocity is equal to:

$$u_N(x,y,z,t) = -\frac{\partial h}{\partial x}\left(\frac{\Delta\rho\, g}{\mu}\right)\frac{1}{2}\left[\left(\frac{b_0 x^k z^r}{2}\right)^2 - y^2\right],$$
$$\text{for } \left(\frac{2|y|}{b_0 x^k}\right)^{1/r} \le z \le h,\ |y| \le \frac{b_0 x^k z^r}{2}, \quad (4)$$

after imposing the nonslip condition at the walls $y = \pm(b_0/2)x^k z^r$ and the null shear stress condition in the midplane $y = 0$, $\tau_{yx}|_{y=0} = 0 \to \partial u/\partial y|_{y=0} = 0$. Averaging the velocity in the z and y directions yields

$$\overline{u}_N(x,t) = -\frac{\partial h}{\partial x}\left(\frac{b_0 x^k}{2}\right)^2\left(\frac{\Delta\rho\, g}{\mu}\right)\beta_N(r)h^{2r}, \quad \beta_N(r) = \frac{r+1}{3(3r+1)}. \quad (5)$$

In the second case, for the wide flow model, the streamwise velocity is equal to:

$$u_W(x,y,z,t) = -\frac{\partial h}{\partial x}\left(\frac{\Delta\rho\, g}{\mu}\right)\frac{1}{2}\left[\left[h - \left(\frac{2y}{b_0 x^k}\right)^{1/r}\right]^2 - (h-z)^2\right],$$
$$\text{for } \left(\frac{2|y|}{b_0 x^k}\right)^{1/r} \le z \le h,\ |y| \le \frac{b_0 x^k z^r}{2}, \quad (6)$$

after imposing the nonslip condition at the walls $y = \pm(b_0/2)x^k z^r$ and the null shear stress condition at the interface with the ambient fluid $z = h$, $\tau_{zx}|_{z=h} = 0 \to \partial u/\partial z|_{z=h} = 0$, since the ambient fluid viscosity has negligible effects. Averaging the velocity in the z and y directions yields

$$\overline{u}_W(x,t) = -\frac{\partial h}{\partial x}\left(\frac{\Delta\rho\, g}{\mu}\right)\beta_W(r)h^2, \quad \beta_W(r) = (r+1)\mathrm{B}\left[3, 1+r\right], \quad (7)$$

where B[...] is the beta function.

Both models lead to adequately correct results in the domain in which the assumptions are valid.

If the gradients of the tangential stresses along z and y are of the same order of magnitude, we can adopt the Darcy-Weisbach flow resistance equation, where the streamwise cross-section averaged velocity can be expressed as

$$\overline{u}_G = \left(\frac{2g' R_h J}{f}\right)^{1/2}, \quad (8)$$

where $g' = (\Delta\rho/\rho)g$ is the reduced gravity, $R_h = A/P$ is the hydraulic radius, i.e. the ratio between the cross-sectional area of the current A and the wetted perimeter P (the total length of channel walls in contact with the liquid); J is the energy grade, energy dissipation per unit weight of fluid and per unit path length; and f is the Fanning friction factor. See, e.g., Chow[20] for a more thorough definition of hydraulics terminology.

In the laminar viscous regime, $f = K/\mathrm{Re}$, where Re is the Reynolds number and K is a numerical coefficient that depends on the shape of the cross-section. The Reynolds number for Newtonian fluids is defined as

$$\mathrm{Re} = \frac{4\rho \overline{u}_G R_h}{\mu}, \tag{9}$$

where ρ is the density and μ is the dynamic viscosity.

In uniform flow, $J = -\partial h/\partial x$, eq. (8) becomes

$$\overline{u}_G = -\frac{\partial h}{\partial x}\left(\frac{\Delta\rho\, g}{\mu}\right)\frac{8}{K}R_h^2. \tag{10}$$

The numerical value of the coefficient K can be calculated analytically for circular ($K = 16$), rectangular ($K = 14.227 - 24.0$ for square ducts and very wide cross-section) and triangular symmetric sections ($K = 12.474 - 13.153$ as a function of the angle)[21] in the presence of Newtonian fluids. These values have been verified experimentally and are in the range 12-24. For a rectangular cross-section ($r = 0$) with $W \ll h$ (narrow flow), the hydraulic radius equals half the local width, $R_h = b_0 x^k/2$, and comparing eq. (5) and eq. (10) yields $K = 24$. If the flow in the rectangular cross-section is wide, with $W \gg h$, the hydraulic radius equals the height of the current, $R_h = h$, and comparing eq. (7) and eq. (10), again yields $K = 24$.

The structure of the Darcy-Weisbach equation has been validated with several other cross-sections by numerically solving eq. (2), see Shah & London[21]. This means that the solution can be considered "exact" with a constant value of K independent of the Reynolds number. However, a possible source of error could be the variation of K as the degree of filling of the cross-section changes.

The hydraulic radius for a cross-section with the boundaries described by $y = (b_0/2)x^k z^r$

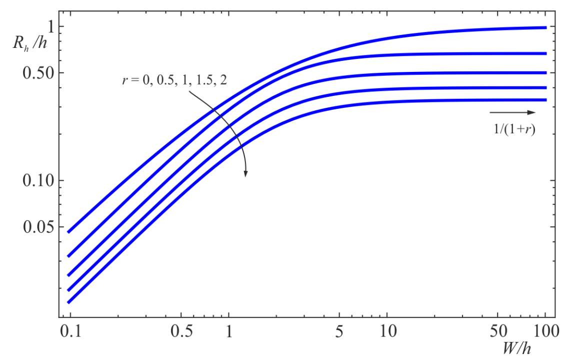

FIG. 2. Ratio $\chi = R_h/h$ between the hydraulic radius and the height h of the current for different values of r as a function of W/h, where W is the top width of the current.

is expressed as $R_h = h\chi(\zeta, r)$, where χ is a dimensionless coefficient equal to

$$\begin{cases} \chi = \dfrac{\zeta}{(r+1)\sqrt{1+\zeta^2} + (r^2-1)\,{}_2\mathrm{F}_1\left[\dfrac{1}{2}, \dfrac{1}{2r-2}, 1+\dfrac{1}{2r-2}, -\zeta^2\right]}, \text{ if } r > 1, \\ \\ \chi = \dfrac{\zeta^2(2-r)}{(r+1)(2-r)\zeta\sqrt{1+\zeta^2} + (r^2-1)\,{}_2F_1\left[\dfrac{1}{2}, \dfrac{r-2}{2(r-1)}; \dfrac{4-3r}{2-2r}; -\dfrac{1}{\zeta^2}\right]}, \text{ if } 0 \le r \le 1, \end{cases} \tag{11}$$

where $\zeta = r(W/h)/2$, $W = b_0 x^k h^r$ is the top width of the current and ${}_2\mathrm{F}_1[\ldots]$ is the hypergeometric function.

Figure 2 shows the coefficient $\chi = R_h/h$ as a function of W/h for different values of r. The asymptotic value for $W/h \to \infty$ is equal to $1/(1+r)$; hence, the computed flow resistance for a given gradient pressure is generally higher if the hydraulic radius is considered instead of the height of the current, with a higher flow depth and a reduced speed of the current.

Substituting the expression for the hydraulic radius in eq. (10) yields

$$\overline{u}_G(x,t) = -\frac{\partial h}{\partial x}\left(\frac{\Delta\rho\, g}{\mu}\right)\beta_G(K)h^2\chi^2, \quad \beta_G(K) = \frac{8}{K}. \tag{12}$$

The continuity equation for the channel is

$$\frac{\partial A}{\partial t} + \frac{\partial(Au)}{\partial x} = 0, \tag{13}$$

which, for a power function cross-section, becomes

$$\frac{\partial h^{r+1}}{\partial t} + \frac{1}{x^k}\frac{\partial(x^k h^{r+1} u)}{\partial x} = 0, \tag{14}$$

where, for simplicity, we have eliminated the overline for the variable u.

At this point, we can check that a self-similar solution of the first kind exists for flow from the origin, with positive velocity; see Longo *et al.*[22].

For flows towards the origin, with negative velocity, an analytical scaling of the variables to combine them in self-similar form is not available. A possible solution for the two cases of narrow and wide flow models consists of searching for a self-similar solution of the second kind. Here, we consider the case of a wide flow model first; the case of a narrow flow model has already been treated in Longo[23] and is briefly described in Appendix A. Then, we consider a cross-section where both tangential stresses are relevant, and the cross-section average velocity of the current is expressed by eq. (12).

B. The wide flow model

For the case of a wide flow model, following the phase space analysis detailed in Gratton & Minotti[5] and the procedure described in Zheng *et al.*[6], we assume that the variables u and h scale as

$$\begin{cases} u_W(x,t) = \dfrac{x}{t_r} U(x,t_r), & (15a)\\[2mm] h(x,t) = \left(\dfrac{\mu}{\Delta\rho\, g}\right)^{1/3} \dfrac{1}{t_t |t_r|^{-2/3}} \left(\dfrac{x^2 H(x,t_r)}{\beta_W}\right)^{1/3}, & (15b)\end{cases}$$

where $t_r = t_c - t$ and t_c is the closure or touchdown time (time when the front of the current reaches the origin) and where U and H are dimensionless. A positive t_r refers to the preclosure phase, with part of the channel still dry, and a negative t_r refers to the postclosure or levelling phase, with the entire channel occupied by the current and the fluid progressively filling up to a horizontal uniform level. Inserting eqs. (15a–15b) into eqs. (7–14) yields

$$\begin{cases} 3U + 2H + x\dfrac{\partial H}{\partial x} = 0, & (16a)\\[2mm] (r+1)H - (r+1)t_r\dfrac{\partial H}{\partial t_r} + 3xH\dfrac{\partial U}{\partial x} & \\ \qquad + (r+1)xU\dfrac{\partial H}{\partial x} + HU[3(k+1) + 2(r+1)] = 0. & (16b)\end{cases}$$

Define the dimensionless variable $\xi = x/(l t_r |t_r|^{\delta-1})$, where l is a coefficient having dimension $[l] = LT^{-\delta}$ and where δ is the unknown exponent to be determined as a part of the solution, and insert it into eqs. (16a–16b), to yield

$$\begin{cases} 3U + 2H + \dfrac{\mathrm{d}H}{\mathrm{d}\,\ln\xi} = 0, & \text{(17a)} \\ (r+1)H + \delta(r+1)\dfrac{\mathrm{d}H}{\mathrm{d}\,\ln\xi} + 3H\dfrac{\mathrm{d}U}{\mathrm{d}\,\ln\xi} \\ \qquad + (r+1)U\dfrac{\mathrm{d}H}{\mathrm{d}\,\ln\xi} + HU[3(k+1) + 2(r+1)] = 0, & \text{(17b)} \end{cases}$$

where the symbol of partial derivative is changed to total derivative since H and U are a function of ξ only. Equations (17a–17b) can be written as

$$\begin{cases} \dfrac{\mathrm{d}H}{\mathrm{d}U} = \dfrac{3H(3U+2H)}{g(H,U)}, & \text{(18a)} \\ \dfrac{\mathrm{d}\ln\xi}{\mathrm{d}H} = -\dfrac{1}{3U+2H}, & \text{(18b)} \\ \text{where} \quad g(H,U) = H[3(k+1)U - 2\delta(r+1) + r + 1] \\ \qquad\qquad - 3(r+1)(\delta+U)U. & \text{(18c)} \end{cases}$$

Equations (18a–18b) are an autonomous system of ordinary differential equations (ODEs) where the solutions are represented by paths in the phase space $U-H$ connecting two singular points that correspond to the boundary conditions. By setting the numerator and denominator of eq. (18a) to zero and infinity, respectively, we find six singular points. The three points in the following list are finite:

$$\begin{cases} \mathrm{O}:(H,U) \equiv (0;0), & \text{(19a)} \\ \mathrm{A}:(H,U) \equiv (0;-\delta), & \text{(19b)} \\ \mathrm{B}:(H,U) \equiv \left[\dfrac{3(r+1)}{2(5+2r+3k)}; -\dfrac{r+1}{5+r(3k+1)}\right]. & \text{(19c)} \end{cases}$$

The other three points are at infinity:

$$\begin{cases} \mathrm{C}:(H,U) \equiv \left[-\infty; \dfrac{(r+1)(2\delta-1)}{3(k+1)}\right], & \text{(20a)} \\ \mathrm{D}:(H,U) \equiv (0;\infty), & \text{(20b)} \\ \mathrm{E}:(H,U) \equiv (\infty;\infty). & \text{(20c)} \end{cases}$$

Points O and A represent the relevant boundary conditions for a GC that, at the front $x = x_f$, has null height and advances with a dimensionless velocity $U = -\delta$ (see Gratton

& Minotti[5]); hence, the integral path during the preclosure phase should connect O and A. The approximate integral curve in the neighbourhood of O during the preclosure phase ($H > 0$ and $U < 0$) is

$$U \approx -\frac{2\delta - 1}{3\delta} H, \tag{21}$$

which requires $\delta > 1/2$. The approximate integral curve in the neighbourhood of A is

$$U \approx \frac{[\delta(k+2) + (\delta - 1)r - 1] + \delta(2k + r + 3)}{3\delta(r+4)} H - \delta, \tag{22}$$

which requires $\delta > (r+1)/(5 + 2r + 3k)$; this last condition is always satisfied if $\delta > 1/2$.

Point C represents the origin in an asymptotic spreading GC with no inflow at the origin; hence, the integral path connecting O and C describes the postclosure (levelling) phase. In the neighbourhood of C, the approximate integral curve is

$$U \approx \frac{(r+1)U_C(\delta + U_C)}{(3+k)} \frac{1}{H} + U_C, \tag{23}$$

where U_C is the velocity in C.

The other points are not of specific interest for the present analysis.

1. *Integration of the ODEs*

Integration of eq. (18a) was performed in Mathematica[24] for the preclosure phase, with the function **NDSolve**. The fastest way to perform the calculations consists of (i) integration starting nearby O, in the quadrant $U < 0, H > 0$ for U in the interval $[-\epsilon, -1.1(\delta/2)]$ with $\epsilon = 10^{-3} - 10^{-4}$, tracing the first partial solution $H^+(U, \delta)$; (ii) integration starting nearby A, for U in the interval $[-0.9(\delta/2), -\delta + \epsilon]$, again with $\epsilon = 10^{-3} - 10^{-4}$, tracing the second partial solution $H^-(U, \delta)$. The two solutions $H^+(U, \delta)$ and $H^-(U, \delta)$ are parametric in the unknown δ; therefore, with the **FindRoot** algorithm, we find the value of δ such that $H^+(-\delta/2, \delta) = H^-(-\delta/2, \delta)$. The algorithm is quite fast and allows the critical eigenvalue δ_c (i.e., the value of the exponent δ that allows to satisfy the differential problem) to be calculated with the desired accuracy.

Figure 3 shows the critical eigenvalues computed for varying r and k. The values for $r = 0$ and $k = 1$ correspond to an axisymmetric converging GC, with the critical eigenvalue $\delta_c = 0.762035$ already computed in Longo *et al.*[15].

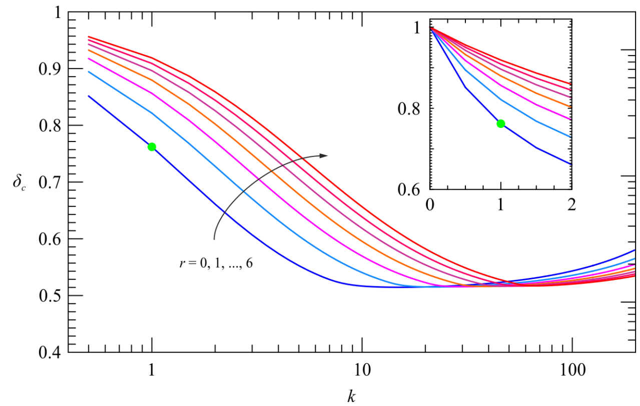

FIG. 3. Eigenvalues for a Newtonian fluid advancing towards the origin of a channel of width $b = b_0 x^k z^r$, for $r = 0, 1, ..., 6$. The green symbol corresponds to δ_c for an axisymmetric GC. The inset shows the critical eigenvalues for $k \to 0$.

The postclosure (levelling) branch can be integrated directly from the expansion in the neighbourhood of point C of eq. (18a), making use of the δ_c eigenvalue identified for pre-closure. For both phases, the calculation of $H(U)$ is followed by the calculation of $\xi(U)$ by integrating eq. (18b). By inversion, $U(\xi)$ and $H(\xi)$ are obtained. Figure 4 shows the integral paths for two different groups of parameters. The scenario is identical for different groups of parameters, except for the scaling of the critical points.

Figure 5 shows the dimensional profiles of the GC computed for different combinations of the parameters. Note that the faster the front is, the greater r, as is evident from figure 3 at least for $k < 10$. It is intuitive, since a cross-sectional width that grows faster with z favours less drag.

The analysis of the expansion of the differential problem near the critical points gives an indication of the range of variability of the eigenvalues. Inserting the expansion of H near the origin, eq. (21), into eq. (18b) and integrating, yields

$$H \approx C\xi^{-1/\delta_c}, \tag{24}$$

and, in dimensional variables

$$h \propto x^{(2\delta_c - 1)/(3\delta_c)}, \tag{25}$$

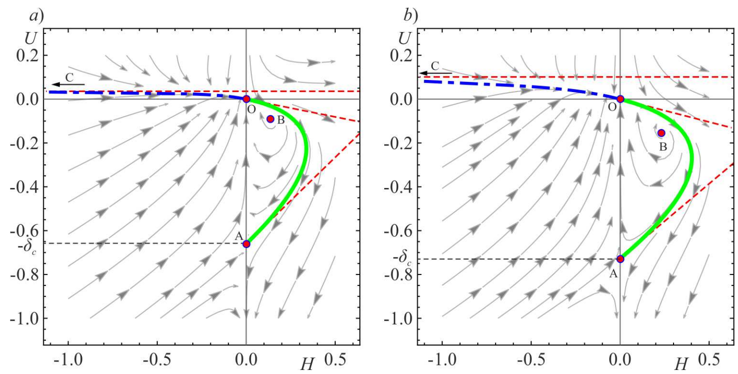

FIG. 4. Integral path for a GC of a Newtonian fluid advancing in a converging channel with $k = 2$, a) in a rectangular cross-section ($r = 0$), and b) in a triangular cross-section ($r = 1$). The continuous green curve refers to the preclosure phase, and the dash-dotted blue curve refers to the levelling phase. The dash-dotted curves represent the expansion in the neighbourhood of the critical points. The scenario is repeated identically for each parameter combination, and only the positions of the critical points are different.

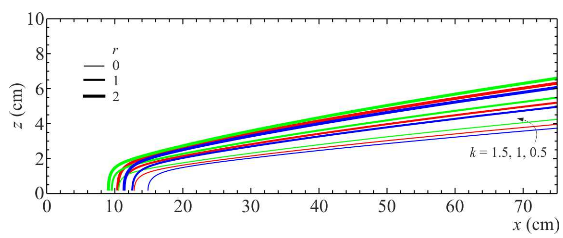

FIG. 5. Computed profiles of the current with the front position at $t_r = 5\,\mathrm{s}$. The profiles refer to a current with the front position $x_f = 75\,\mathrm{cm}$ at $t_r = 50\,\mathrm{s}$ for different combinations of the parameters r and k. The fluid is Newtonian with viscosity $\mu = 0.5\,\mathrm{Pa\,s}$ and $\Delta\rho = 1256\,\mathrm{kg\ m^{-3}}$.

which is time independent. Since $\mathrm{d}h/\mathrm{d}x > 0$, for $x \to \infty$, the results again show that $\delta_c > 1/2$. Inserting the expansion of H near the asymptotic critical point C, eq. (23), into eq. (18b) and integrating yields

$$H \approx C\xi^{-2}, \tag{26}$$

and, in dimensional variables,

$$h \propto (-t_r)^{(-2\delta_c-1)/3}, \tag{27}$$

which is space independent. The negative sign for t_r stems from the fact that we are in the levelling phase, with $t_r < 0$. Imposing that during the levelling phase the condition $\mathrm{d}h/\mathrm{d}t > 0$, equivalent to $\mathrm{d}h/\mathrm{d}t_r < 0$, yields $\delta_c < 1$. The combination of the constraints on the critical eigenvalue gives $1/2 < \delta_c < 1$.

The dimensional speed and acceleration of the front are equal to

$$u_f = -\frac{x_0}{t_c}\delta_c\left(1-\frac{t}{t_c}\right)^{\delta_c-1}, \quad a_f = \frac{x_0}{t_c^2}\delta_c(\delta_c-1)\left(1-\frac{t}{t_c}\right)^{\delta_c-2}, \tag{28}$$

where x_0 is the front position at time $t = 0$. For $\delta_c > 1$, the front of the current accelerates, i.e., the modulus of the negative front speed decreases, while for $\delta_c < 1$, the opposite is true. The wide flow model always predicts decelerated currents (the front speed increases in time), while the narrow flow model predicts accelerated currents except for $r > 0$, where it admits a deceleration for small k.

C. The general model (Darcy-Weisbach)

In the case where none of the tangential stresses is dominant, the analysis of the propagation of the current leads to a differential problem not admitting a self-similar solution, which requires numerical integration. We do not expect a self-similar behaviour, since the structure of the equation precludes the identification of a group of transformations in which it is invariant.

Inserting eq. (12) in eq. (14) yields

$$\frac{\partial h^{r+1}}{\partial t} = \frac{1}{x^k}\frac{\partial}{\partial x}\left[\left(\frac{\Delta\rho\, g}{\mu}\right)\beta_G(K)\chi^2 x^k h^{r+3}\frac{\partial h}{\partial x}\right]. \tag{29}$$

If we select the following velocity and time scales:

$$u^* = \frac{8}{K}\left(\frac{\Delta\rho\, g}{\mu}\right)\frac{h^{*3}}{L}, \quad t^* = \frac{L}{u^*}, \tag{30}$$

where L and h^* are the horizontal and vertical length scales, respectively, eq. (29) can be written in dimensionless form as

$$\frac{\partial \widetilde{H}^{r+1}}{\partial \widetilde{T}} = \frac{1}{\widetilde{X}^k}\frac{\partial}{\partial \widetilde{X}}\left[\chi^2 \widetilde{X}^k \widetilde{H}^{r+3}\frac{\partial \widetilde{H}}{\partial \widetilde{X}}\right], \tag{31}$$

where $\widetilde{H} = h/h^*$, $\widetilde{X} = x/L$, $\widetilde{T} = t/t^*$. The coefficient χ is expressed by eqs. (11) but with a dimensionless argument computed as follows. The ratio between the top width of the current and the height can be expressed as $\widetilde{b}_0 \widetilde{X}^k \widetilde{H}^{r-1}$ with

$$\widetilde{b}_0 = b_0 L^k h^{*r-1}, \tag{32}$$

Hence, the dimensionless value for ζ is $\widetilde{\zeta} = r\widetilde{b}_0 \widetilde{X}^k \widetilde{H}^{r-1}/2$.

The mass conservation in integral dimensional form for the simple case of a constant volume of the current is

$$\int_{x_f}^{L} \frac{b_0}{r+1} x^k h^{r+1}\, \mathrm{d}x = V_0, \tag{33}$$

where V_0 is the fluid volume; the corresponding dimensionless formulation reads

$$\int_{\widetilde{X}_f}^{1} \widetilde{X}^k \widetilde{H}^{r+1}\, \mathrm{d}\widetilde{X} = \widetilde{V}_0, \tag{34}$$

where $\widetilde{V}_0 = (r+1)V_0/(\widetilde{b}_0 h^{*2} L)$.

The boundary conditions are

$$\widetilde{H}(\widetilde{X}_f) = 0, \quad \left.\frac{\partial \widetilde{H}}{\partial \widetilde{X}}\right|_{\widetilde{X}=1} = 0, \tag{35}$$

where $\widetilde{X}_f$ is the dimensionless front position.

The integration is performed with an explicit predictor-corrector scheme on a staggered uniform grid, with the nonlinear terms calculated at intermediate points, starting with the following initial condition:

$$\widetilde{H}(\widetilde{X}, 0) = a\left(\frac{\widetilde{X} - \widetilde{X}_{f0}}{1 - \widetilde{X}_{f0}}\right)^s, \quad \widetilde{X}_{f0} < \widetilde{X} < 1, \tag{36}$$

where a and s are dimensionless and $\widetilde{X}_{f0}$ is the initial front position. A sensitivity analysis showed that a grid of 200 points guarantees grid-independent results, with an initial integration interval of $\Delta\widetilde{T} = 10^{-5}$ progressively increasing at a later stage of propagation of the current. Most computations were performed with a grid of 400 points to achieve an adequate resolution of the front position.

Figure 6 shows the GC profiles calculated at different times, with closure at $\widetilde{T} = 4.119$.

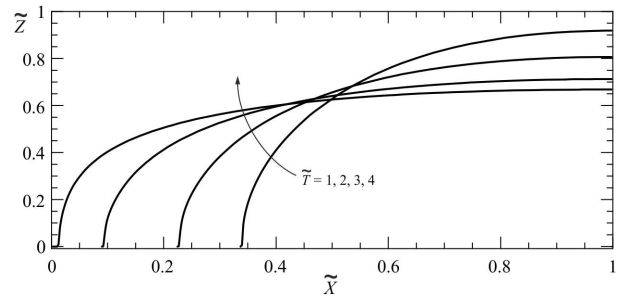

FIG. 6. Non-dimensional profiles of the GC as a result of the finite difference integration for the general model. Newtonian fluid in a converging channel with $r = 0$, $k = 0.5$, $\widetilde{b}_0 = 1$; grid with 400 knots and $\Delta\widetilde{T} = 10^{-5}$.

III. COMPARISON OF THE RESULTS FOR DIFFERENT FLOW RESISTANCE MODELS

Figure 7 shows the critical eigenvalues predicted by the narrow- and wide-flow models. For $k \to 0$ and $r = 0$, both models predict $\delta_c = 1$; for $r > 0$, the wide flow model predicts $\delta_c = 1$, while the narrow flow model predicts $\delta_c < 1$. This means that the choice of the model has little effect on the result for small values of k, i.e., for flows advancing in channels with a limited convergence index, while it makes a large difference for increasing values of k. The green bullets are the points where the two models share the critical eigenvalue $\delta_c \approx 1$ for $r = 0, 0.1, ..., 0.5$. The narrow flow model diverges for $k \to 1$, while the wide flow model always predicts a finite δ_c.

Figure 8 shows the front position versus time for a converging GC of a Newtonian fluid advancing in a rectangular cross-section channel with $r = 0, k = 0.1, 1.2, 3.0$. The continuous and dashed curves refer to the assumption of $u = u_G$ and $u = u_W$, respectively, and the starting current profile is parabolic in the range $0.7 < X < 1$, with $X_{f0} = 0.7$. For comparison, self-similar solutions with $\delta_c = 0.963..., 0.736..., 0.607...$ are shown. There is a fairly good correspondence between the self-similar solution and the result of the numerical finite difference integration for a wide flow, with a progressive adjustment of the solution after a suitable time interval from the start of the simulation. The results for the case of a general model, where the hydraulic radius controls the flow resistance, indicate that there is a wide range in which the dependence of the position of the current front on time is similar

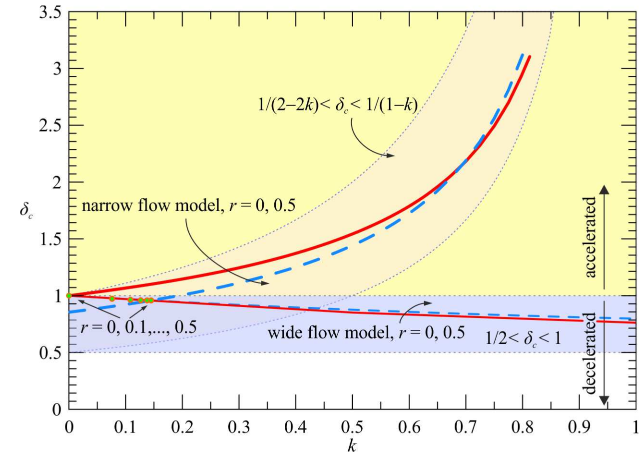

FIG. 7. Critical eigenvalues predicted by the narrow and wide flow models. The continuous and dashed curves refer to $r = 0$ and $r = 0.5$, respectively. The green bullets indicate the common critical eigenvalues for the two models for $r = 0, 0.1, ..., 0.5$. The yellow hatched area is for accelerated flows, with a reduction in the modulus of the negative velocity of the front. The other two hatched areas indicate the range of allowed variability of the critical eigenvalue.

to that predicted by the self-similar solution, although the differences are evident mainly in the early stage, when the initial condition still affects the propagation dynamics, and in the late stage, when the front is reaching the origin.

Similar results are obtained for different shapes of the cross-section; see figure 9. This evidence, albeit numerical, indicates that the approach of finding a self-similar solution appears to be advantageous because the flow resistance law plays a minor role in many configurations. Apart from the numerical value of the coefficients, what most distinguishes the propagation with a general flow resistance law from the simplified case of narrow and wide flow models, is the joint presence in the diffusion term of eq. (31) of the hydraulic radius and the height of the current, where the former is implemented with a quadratic exponent and the latter with an exponent equal to $r+1$; the flow resistance law for currents in narrow or wide flows only considers the height of the current.

The hydraulic radius for a cross-section in power function form depends on the ratio of the top width to the current height, a value that in dimensionless form is closely related to $\widetilde{b}_0$.

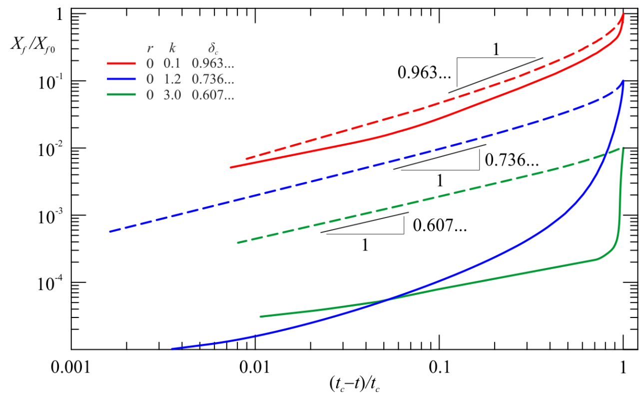

FIG. 8. Converging GC of a Newtonian fluid in a channel of gap width $b = b_0 x^k z^r$, with $r = 0$ (rectangular cross-section), $k = 0.1, 1.2, 3.0$ and $\widetilde{b}_0 = 1$. Comparison between the front position computed by finite difference integration assuming that $u = u_W$ (dashed curves) and assuming that $u = u_G$ (continuous curves). The self-similar solutions (represented by the straight black lines) have critical eigenvalues $\delta_c = 0.963..., 0.736..., 0.607...$. The curves are scaled in the vertical direction for better visualization.

For increasing values of $\widetilde{b}_0$, the hydraulic radius tends to approach its maximum asymptotic value faster. This value coincides with the height for the rectangular cross-section ($r = 0$), i.e., it tends to $h/(1+r)$ for a generic value of r, see figure 2. Figure 10 shows the results of finite difference numerical integration for a rectangular cross-section and for increasing values of $\widetilde{b}_0$, corresponding to an average hydraulic radius that is increasingly close to the height of the GC. Although the results differ, an average slope not dissimilar to that predicted by the self-similar solution for the wide flow model can be observed.

Figure 11 shows the results of the finite difference integration of the three models and the self-similar solution. The values of the parameters refer to the last of the green bullets visible in figure 7, which correspond to an equal critical eigenvalue for both the wide- and narrow-flow models. The results show a good overlap between the three models and the self-similar solution.

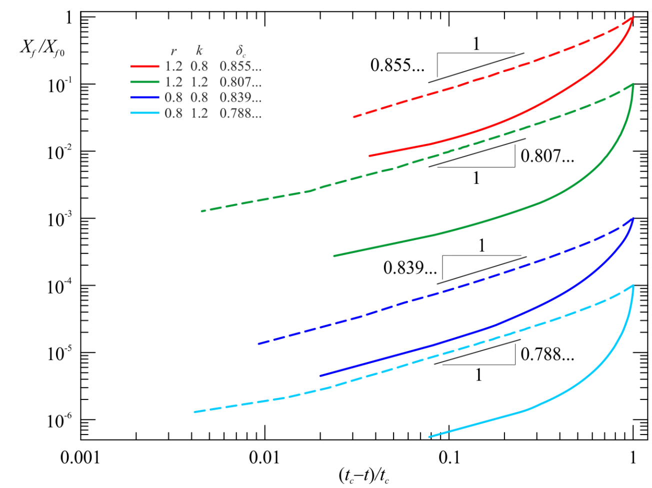

FIG. 9. Converging GC of a Newtonian fluid in a channel of gap width $b = b_0 x^k z^r$, with $r = 0.8 - 1.2$, $k = 0.8 - 1.2$ and $\widetilde{b}_0 = 1$. Comparison between the front position computed by finite difference integration assuming that $u = u_W$ (dashed curves) and $u = u_G$ (continuous curves). The self-similar solutions (represented by the straight black lines) have critical eigenvalues $\delta_c = 0.855..., 0.807..., 0.839..., 0.788$. The curves are scaled in the vertical direction for better visualization.

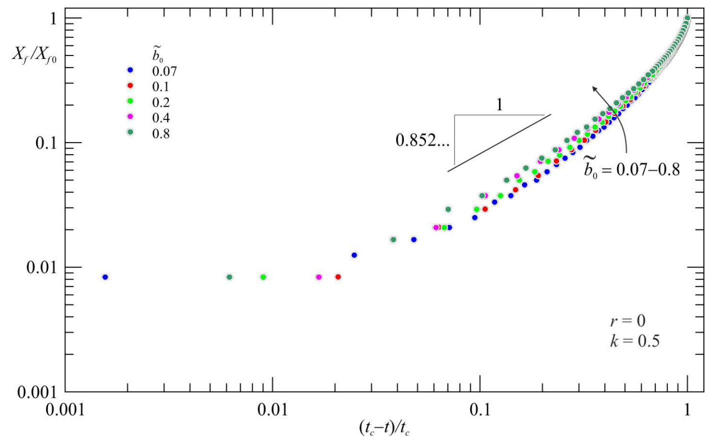

FIG. 10. Converging GC of a Newtonian fluid in a channel of gap width $b = b_0 x^k z^r$, with $r = 0$, $k = 0.5$ and $\widetilde{b}_0 = 0.07 - 0.8$. The symbols are the numerical results for the general model. For comparison, the slope predicted by the self-similar solution of the wide flow model is shown (straight black line).

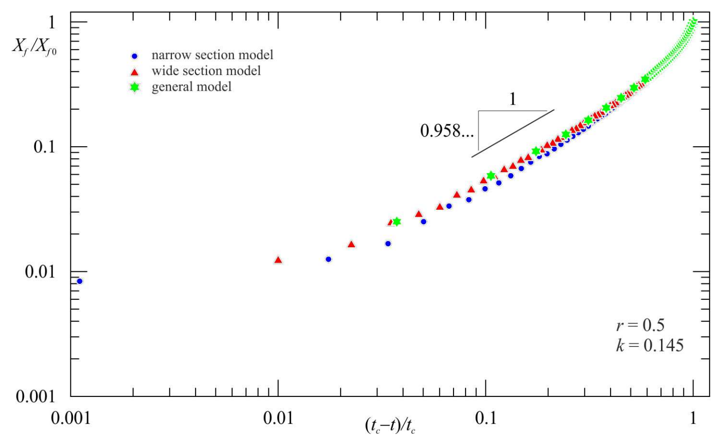

FIG. 11. Converging GC of a Newtonian fluid in a channel of gap width $b = b_0 x^k z^r$, with $r = 0.5$ and $k = 0.145$. The results of the numerical integration for the three models and the self-similar solution (straight black line), with a common critical eigenvalue $\delta_c = 0.958...$, are shown.

IV. SUMMARY AND CONCLUSION

We analysed the behaviour of converging viscous currents in channels with the boundary described by a power function, adopting three different flow resistance models, namely, (i) a wide flow model (new and original), (ii) a narrow flow model, and (iii) a general model (new and original in its application to a GC in a generic power function cross-section). We assume that the cross-section is convergent towards the origin and has a varying width in the vertical direction. This last aspect is new and original.

(i) Previous analyses, conducted for converging GCs both for Newtonian fluids and power-law fluids with a narrow flow model and gap width $b \sim x^k$, led to a self-similar solution of the second kind, with experimental validation[6,9,15]. With the same narrow flow model, a self-similar solution of the second kind also reproduces the case where the cross-section varies vertically, with gap width $b \sim x^k z^r$; see Longo[23]. The critical eigenvalue for the narrow flow model is in the range $1/(2-2k) < \delta_c < 1/(1-k)$ for Newtonian fluids, and the parameter r, which controls the variation of the section in the vertical direction, does not intervene in the definition of this range. Note that the critical eigenvalue increases with k, and that for $k \to 1$ the critical eigenvalue tends to infinity, a singularity presumably due to the inappropriateness of the scheme when the channel walls diverge more than linearly. The converging GCs framed in a narrow flow model are generally accelerated, with the negative front velocity reducing the modulus during propagation. When $r > 0$ and for sufficiently small k, the flows are decelerated.

(ii) Here, we demonstrate that the wide flow model also leads to a self-similar solution of the second kind. The critical eigenvalue is in the range $1/2 < \delta_c < 1$ for Newtonian fluids. Conversely, this implies that the converging currents framed in the wide flow model are always decelerated, with the negative front velocity increasing in modulus during propagation, although with a deceleration approaching zero. The wide flow model has so far only been applied to the case of converging circular GCs, for which axial symmetry dictates, within the limits of approximations, that the most relevant stress gradient is that in the vertical direction, i.e. a dominant dynamics in the vertical. The extension to the case of flows in converging channels (coinciding with those with axial symmetry for $k = 1$ and $r = 0$) shows that the critical eigenvalues decrease as k

increases and that are always bounded and without singularities.

(iii) The general model leads to a nonlinear differential diffusion equation that does not admit a self-similar solution. However, numerical integration shows that the evolution of the front follows to some extent that predicted by the self-similar solution, except for the initial and final phases of propagation.

In particular, for $r \lesssim 0.5$ and for small values of k, the three models tend to give very similar results, with $\delta_c \approx 1$ for the two self-similar solutions.

The results provide a fairly clear perspective on the interpretation of experimental results compared to theoretical models. In fact, GCs very often propagate partly according to the narrow flow model and partly according to the wide flow model, and only very rarely can their dynamics be attributed to a single specific model. Nevertheless, the experimental results are generally in good agreement with the theory. This is apparently also because the general model reproduces fairly well the results of the narrow and wide flow models to a greater or lesser degree of approximation, and the expected approximation is better for smaller the value of k and r.

The mathematical results appear to be quite consistent and coherent, but an experimental verification is needed. In this sense, the recommendations in Ghodgaonkar[25] on the need to design experiments in such a way as to extend the time interval between t_{sim}, the onset of self-similarity, and the touchdown time t_c, point to the desirability of more rigorous experimental validation, with experiments that are clearly framed in one of the two regimes that allow self-similarity.

DECLARATION OF INTERESTS

The author reports no conflict of interest.

V. ACKNOWLEDGEMENTS

This project was funded under the National Recovery and Resilience Plan (NRRP), Mission 4 Component 2 Investment 1.5 – Call for tender No. 3277 of 30/12/2021 of the Italian Ministry of University and Research funded by the European Union – NextGenerationEU.

Project code ECS00000033, Concession Decree No. 1052 of 23/06/2022 adopted by the Italian Ministry of University and Research, CUP D93C22000460001, "Ecosystem for Sustainable Transition in Emilia-Romagna" (Ecosister), Spoke 4.

AUTHOR DECLARATIONS

Conflict of Interest

The author has no conflicts to disclose.

DATA AVAILABILITY STATEMENT

Data sharing is not applicable to this article, as no new data were created or analysed in this study.

Appendix A: The analysis for a narrow flow model

Using the same methodology as that used for the wide flows, we obtain the following system of ODEs:

$$\begin{cases} \dfrac{\mathrm{d}H}{\mathrm{d}U} = \dfrac{H|H|^{4r}[2(1-k)H|H|^{2r} + (2r-1)U]}{H|H|^{2r}[(k+1)(2r-1)U - 2(1-k)(r+1)\delta + r + 1] - (r+1)(U+\delta)(2r-1)U}, \\ \dfrac{\mathrm{d}\ln\xi}{\mathrm{d}H} = -\dfrac{(2r-1)}{H|H|^{2r-1}(2r-1)U + 2(1-k)H|H|^{4r}}. \end{cases} \tag{A1}$$

The analysis and the procedure for the solution are the same as that for wide flows.

REFERENCES

[1] G. I. Barenblatt and Y. B. Zel'Dovich, "Self-similar solutions as intermediate asymptotics," Annual Review of Fluid Mechanics **4**, 285–312 (1972).

[2] S. Longo, *Principles and applications of dimensional analysis and similarity* (Springer, 2021).

[3]M. Ungarish, *Gravity Currents and Intrusions – Analysis and Prediction* (World Scientific, 2020).

[4]H. E. Huppert, "Flow and instability of a viscous current down a slope," Nature **300**, 427–429 (1982).

[5]J. Gratton and F. Minotti, "Self-similar viscous gravity currents: phase-plane formalism," Journal of Fluid Mechanics **210**, 155–182 (1990).

[6]Z. Zheng, I. C. Christov, and H. A. Stone, "Influence of heterogeneity on second-kind self-similar solutions for viscous gravity currents," Journal of Fluid Mechanics **747**, 218–246 (2014).

[7]Z. Zheng, S. Shin, and H. A. Stone, "Converging gravity currents over a permeable substrate," Journal of Fluid Mechanics **778**, 669–690 (2015).

[8]J. A. Diez, J. Gratton, and F. Minotti, "Self-similar solutions of the second kind of non-linear diffusion-type equations," Quarterly of Applied Mathematics **50**, 401–414 (1992).

[9]J. A. Diez, R. Gratton, and J. Gratton, "Self-similar solution of the second kind for a convergent viscous gravity current," Physics of Fluids A: Fluid Dynamics **4**, 1148–1155 (1992).

[10]D. G. Aronson and J. Graveleau, "A selfsimilar solution to the focusing problem for the porous medium equation," European Journal of Applied Mathematics **4**, 65–81 (1993).

[11]S. B. Angenent and D. G. Aronson, "The focusing problem for the radially symmetric porous medium equation," Communications in Partial Differential Equations **20**, 1217–1240 (1995).

[12]S. B. Angenent and D. G. Aronson, "Intermediate asymptotics for convergent viscous gravity currents," Physics of Fluids **7**, 223–225 (1995).

[13]D. G. Aronson, J. B. Van Den Berg, and J. Hulshof, "Parametric dependence of exponents and eigenvalues in focusing porous media flows," European Journal of Applied Mathematics **14**, 485 (2003).

[14]J. Gratton and C. A. Perazzo, "Self-similar collapse of a circular cavity of a power-law liquid," Journal of non-Newtonian Fluid Mechanics **165**, 158–162 (2010).

[15]S. Longo, L. Chiapponi, D. Petrolo, A. Lenci, and V. Di Federico, "Converging gravity currents of power-law fluid," Journal of Fluid Mechanics **918**, A5 (2021).

[16]Z. Zheng and H. A. Stone, "The influence of boundaries on gravity currents and thin films: drainage, confinement, convergence, and deformation effects," Annual Review of

Fluid Mechanics **54**, 27–56 (2022).

[17]T. V. Ball, H. E. Huppert, J. Lister, and J. Neufeld, “The relaxation time for viscous and porous gravity currents following a change in flux,” Journal of Fluid Mechanics **821**, 330–342 (2017).

[18]T. V. Ball and H. E. Huppert, “Similarity solutions and viscous gravity current adjustment times,” Journal of Fluid Mechanics **874**, 285–298 (2019).

[19]D. Takagi and H. E. Huppert, “The effect of confining boundaries on viscous gravity currents,” Journal of Fluid Mechanics **577**, 495–505 (2007).

[20]V.-T. Chow, *Open-Channel Hydraulics* (McGraw Hill, 1988).

[21]R. K. Shah and A. L. London, *Laminar flow forced convection in ducts: a source book for compact heat exchanger analytical data* (Academic press, 2014).

[22]S. Longo, V. Di Federico, and L. Chiapponi, “Propagation of viscous gravity currents inside confining boundaries: the effects of fluid rheology and channel geometry,” Proceedings of the Royal Society of London A: Mathematical, Physical and Engineering Sciences **471** (2015), 10.1098/rspa.2015.0070.

[23]S. Longo, “Gravity currents of viscous fluids in a vertically widening and converging fracture,” Physics of Fluids **35** (2023), 066601.

[24]Wolfram Research, Inc., “Mathematica, Version 13.2.1.0,” (2022), Champaign, IL.

[25]A. A. Ghodgaonkar, *Numerical methods for studying self-similar propagation ov viscous gravity currents*, Master's thesis, Purdue University, West Lafayette, Indiana (2019).